Accepted Manuscript

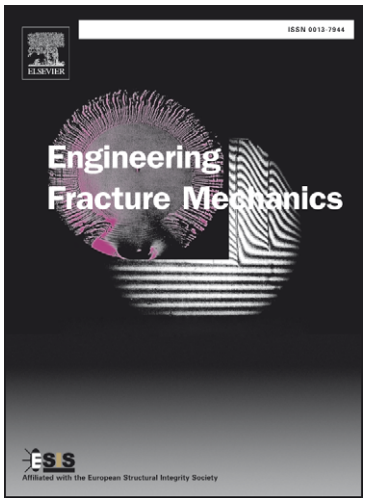

The fracture toughness of an Imperial Roman mortar

P. Brune, A.R. Ingraffea, M.D. Jackson, R. Perucchio

PII: S0013-7944(13)00049-0
DOI: http://dx.doi.org/10.1016/j.engfracmech.2013.02.007
Reference: EFM 3975

To appear in: *Engineering Fracture Mechanics*

Received Date: 10 February 2012
Revised Date: 20 October 2012
Accepted Date: 11 February 2013

Please cite this article as: Brune, P., Ingraffea, A.R., Jackson, M.D., Perucchio, R., The fracture toughness of an Imperial Roman mortar, *Engineering Fracture Mechanics* (2013), doi: http://dx.doi.org/10.1016/j.engfracmech.2013.02.007

The fracture toughness of an Imperial Roman mortar

P. Brune[a], A.R. Ingraffea[b], M.D. Jackson[c], R. Perucchio[a]

[a] Department of Mechanical Engineering, University of Rochester

[b] Civil and Environmental Engineering, Cornell University

[c] Civil and Environmental Engineering, University of California at Berkeley

Abstract.

The vaulted concrete monuments of ancient Rome have an unreinforced concrete core of Pozzolanic mortar and decimeter-sized coarse aggregate. An assessment of the mechanical and fracture properties of a reproduced Trajanic-era (*c*. 100AD) mortar is the subject of the present work. Description of a newly developed arc-shaped three-point bending test, devised to optimize eventual testing of Trajanic-era concrete specimens with an unusual drill core geometry, is supplemented with details of the reproduced material composition and inverse data reduction procedures. Three ages of mortar are tested, with results suggesting a relatively long curing process that increases mechanical and fracture properties. The mortar cured longest (180 days) is found to have a Young's modulus of 3.4GPa, uniaxial tensile strength of 0.5MPa, and mode-I tensile fracture energy of 55J/m^2. These measurements describe a relatively ductile cementitious material with respect to modern concretes.

Keywords: toughness testing; mortar and concrete; cohesive zone modeling, volcanic ash pozzolans.

1. Introduction

Roman concrete forms some of antiquity's largest and toughest structures. Several of these constructions included free spans in excess of twenty meters covered by unreinforced concrete vaults. That some of these monuments survive today is the result of the enduring collaboration

between structural form and constituent material. This resounding success in engineering design is not well understood as such: most of the scholarly attention given to these monuments concerns their architectural or art-historical significance. The few studies [1-5] that have included structural treatments do not incorporate fracture mechanics to describe the mechanical behavior of the concrete. This is necessary to quantify the proximity to failure and thereby meaningfully analyze the vaulted constructions, whose highly three-dimensional forms and self-coherent concrete material discourage the use of rigid-plastic analysis as applied to historical constructions made from jointed masonry (not to be confused with concrete) [6, 7].

An overarching goal of the present study is the analytical representation of the tensile fracture process to enable a better understanding of the structural behavior of Roman vaulted concrete monuments [8]. However, current analytical studies in this regard are limited by a lack of experimental data [9, 10]. The only published results for the tensile resistance of the concrete are two measures of the modulus of rupture from insufficiently large specimens [11]. Otherwise, the testing of Roman concrete core-samples [11, 12] has almost exclusively targeted compressive strength [9]. While compressive strength is of obvious importance for *modern* concrete structures, it is the tensile fracture behavior that is presently considered more relevant to the survival of the spanning structures of ancient Roman vaulted constructions.

We have hypothesized that, in the absence of steel reinforcement, Roman concrete survives tensile loads by inhibiting the formation of structural-scale discontinuities [8]. The material's remarkable service record, however, has yet to motivate the experimental examination of its fracture mechanics. Chief among the obstacles to doing so is the highly heterogeneous meso-scale composition of the concrete material, which consists of decimeter-sized coarse aggregate bonded with a pozzolanic mortar, itself containing up to centimeter-sized scoriaceous volcanic ash aggregate (fig. 1).

The broader experimental program targets a structural-scale description of the tensile fracture process of this multi-scale heterogeneous material. Integral to this, and the subject of this paper, is the Mode-I fracture process of the pozzolanic mortar, composed of hydrated lime and a specific volcanic ash that crops out in the environs of Rome. The mortar is the fundamental binding substance of the concrete, composing around 40 to 50 percent of its total volume and

making critical contributions to its composite mechanical response, particularly in tension. The experiments operate on a mortar mix that is based on the wall concrete formulation [13] from the Great Hall of Trajan's Markets (*c*. 110AD), one of the most durable concrete formulations in human history [14]. The selection of this composition arises from studies [15] that have identified a mix design that accurately reproduces this particular mortar, and from the generous contribution by the Sovraintendenza ai Beni Culturali del Comune di Roma of six 20cm-diameter drill core-samples of the ancient concrete.

The size, shape, and composition (in terms of relative aggregate size) of these drill cores, which have an unusual geometry with a central hole around 5-6cm in diameter (fig. 1a), in conjunction with the very limited availability of ancient material, especially in larger specimens, prompt the usage of an arc-shaped three-point bending fracture test for testing the mortar reproductions (fig. 1b). The newly developed test will allow us to utilize the present experimental results to better understand the role of the mortar in the ancient Great Hall concrete: testing of arc-shaped mortar specimens will be correlatable with results from testing of identical specimen geometries from the ancient core-samples, which will be tested at a later date. A conventional three-point bending test utilizing established methods [16-18], would not allow for such a direct comparison with those future tests of the ancient concrete.

The development of the new fracture test is also a byproduct of material scarcity. Ancient Roman concrete that is available for destructive testing is exceedingly rare. Any authentic material obtained for testing is invaluable and must be utilized to the fullest extent possible. For example, extracting (notched) prismatic elements for use in conventional fracture tests would destroy an unacceptable amount of precious ancient material and produce test specimens of further reduced size. Thus, selecting an arc-shaped geometry for the mortar tests maximizes the size of the specimens and the eventual applicability of test results to the hollow cylindrical shape of the drill core-samples of ancient material, as well as the number of replicates. An additional benefit of the arc-shaped geometry is the smooth inner arc, which concentrates bending tensile stresses to localize the eventual macrofracture without requiring a notch and the associated stress singularity. This permits the simultaneous measurement of the modulus of rupture.

The present testing focuses on the reformulated pozzolanic mortar, and not the ancient concrete cores, for two reasons. First, the novel arc-shaped test requires a thorough development process. The re-formulated mortar is utilized to guarantee a fully functional test system for eventual use with the irreplaceable ancient material. Second, the relatively small size with respect to the large aggregate inclusions (fig. 1a) of the Trajanic cores means that their testing will not directly produce the structural-scale response that is the ultimate objective of the experimental program. Instead, the response of the ancient cores will provide a set of constraints by which to optimize the combination of the individual responses of the large aggregate materials and the pozzolanic mortar – thus the need to test it first – into a composite response, as provisioned in [9].

Finally, it must be noted that the unique provenance of the volcanic ash, excavated from various quarries [8,13] around Rome and transported to Cornell University for casting of test specimens, limited the amount of material that could be fabricated for testing. This prevented the parallel execution of established fracture tests on the reformulated mortar; the utility of doing so is discussed further in section 4.

The reproduction and testing of the Imperial-age (Trajanic) pozzolanic mortar is outlined as follows: first the methods and materials are presented. The experimental results appear next, along with a summary of several data refinement processes. The two-part data reduction process to extrapolate engineering properties and bilinear traction-separation descriptions within the fictitious crack method is then explained. The paper concludes with a reconciliation of results, both with data from other studies and modern cementitious materials.

2. Experimental Materials and Methods

2.1. Materials.

A single mortar mix was developed and tested. Its constituents, as noted above, were selected to reproduce the pozzolanic mortar of the Great Hall of Trajan's Markets wall concrete [13]. A slaked lime paste binder was combined with Pozzolane Rosse volcanic ash pozzolan from quarries surrounding Rome [8,15]. The volumetric proportion of 1:3 lime:*pozzolana*, as recommended by the Roman engineer Vitruvius in passage 2.4.1 of *de Architectura* [19], controlled their respective quantities in the mix design.

Microscopic petrographic observation of concrete core-samples from the Great Hall identified three alteration facies of the Pozzolane Rosse pyroclastic flow, along with a small quantity of sand-sized palagonitic volcanic glass sand. The relative proportions of each were fixed through point-count data [13]. Sieving of previous samples of dried Pozzolane Rosse identified the natural grain-size distribution of the ash from the Castèl di Leva quarry south of Rome [15] (table 1). This distribution included particles up to 6.35mm and controlled the addition of all three alteration facies of Pozzolane Rosse used in the mix, each named after its quarry of origin: Castèl di Leva (80w%), Corcolle (10w%), and Fossignano (5w%) [15]. Ground Tufo Lionato particles (5w%) <0.60mm from the Tor Cervara quarry were also added as palagonitic glass sand. Measurement of the bulk mass density for these grain size distributions of Pozzolane Rosse (1370Kg/m^3) and Tufo Lionato (1110Kg/m^3) facilitated calculation of their allocation quantities in the mix design.

Quicklime was the preferred form of lime. It both allowed for complete control of the water used in the mix and enabled us to closely duplicate the ancient material fabrication process, as described by Vitruvius in sections 2.5.1–2.5.3 of *de Architectura* [19]. Trial-and-error testing found that the pebble-sized quicklime formed a lime paste of suitable stiffness and workability when it was hydrated with water according to a 1:2.1 quicklime:water ratio by weight. Simple volumetric measurements determined that during hydration the lime paste lost about 35% of its volume. Further exploratory trials determined the appropriate ratio of mixing water added along with the dry volcanic ash aggregate mix to be 1:0.15 ash:water by weight.

2.2. Specimen Preparation.

Casting occurred in three steps. First the quicklime was carefully hydrated and mixed manually until the quicklime pebbles (dull white/gray when dry) had been completely incorporated into a uniformly white lime paste. The dry volcanic ash aggregate was then added along with the mixing water. The material was mixed manually until it reached a uniformly dark maroon color. Lastly, the mortar was transferred from the mixing trough into the molds, wherein it was compacted on a vibration table for a duration of eight minutes. Immediately thereafter the molds were sealed with watertight plastic sheeting to create a saturated curing environment.

Test specimens were arcs of 20cm outer diameter, 5cm inner diameter, and 7.5cm depth (fig. 2). This geometry was selected because it corresponds to one half of a 7.5cm-thick slice through the drill core-samples of the ancient wall concrete from the Great Hall (fig. 1), which will be utilized in future testing.

The casting and curing molds were cylinders 20cm tall with the interior compartmentalized to form the central hole and separate the hollow cylinder into two arcs; only saw-cuts across the outer circumference were necessary. The mortars were de-molded two days prior to testing, and sawn into 7.5cm-deep slices. Next, each specimen was photographed, labeled, and precisely characterized dimensionally; the CMOD clip-gauge mounts and strain gauges were also attached (fig. 2). During these operations the specimens were stored in a chamber at approximately 70 F and 30% relative humidity, conditions likely similar to those of the ancient monument during construction. Post-test examination of fracture surfaces revealed no evidence for non-uniform drying.

2.3. Test Procedure.

The reproduced Imperial mortar was tested at 28, 90, and 180 days hydration. Each age group included eight specimens, for a total of twenty-four tests. The test-system was instrumented to measure load, load-point displacement, circumferential strain, and crack-mouth opening displacement (CMOD), this last of which was used as the control measurement for the servo-hydraulic system. The CMOD clip gauge was attached to plastic mounts (fig. 2, a) that increased the gauge's effective range from 0.5cm to 2.5cm without compromising its effectiveness or stiffening the arch ring. The mounts did creep; this small effect was compensated for during testing by installing the clip-gauge and permitting the mounts to creep for ten minutes before beginning each test. This ensured that the creep progressed from stage-1 to stage-2, characterizable by a linear rate, which was utilized in corrections during data reduction. Thus the clip creep did not affect the functioning of the test or its results. Load was applied through a 2.5cm-wide steel helmet, machined to match the curvature of the arc's outer diameter (fig. 2, b). Strain gauges (1.27cm) were attached to the center of the arch ring (fig. 2, c and fig. 3) to measure circumferential strain.

Three-point bending tests were carried out within a highly stiffened load frame and using an MTS 242.02 actuator. Specimens were staged on 0.64cm-thick steel foot-plates that sat atop 2.5cm steel rollers. A conservative span of 12.5cm (fig. 2) was selected, due to uncertainty concerning the reproduced mortar's properties and coherence, particularly for the 28-day specimens. Load was measured with a JDL200lbf (889.64 N) load-cell conditioned by an MTS Flextest SE with a maximum displacement of 254cm and a sensitivity of 2.54E-4cm. Tests of the 28-day specimens were controlled by a specified CMOD increase rate of 0.075cm/600s, while tests of the 90- and 180-day specimens used a rate of 0.100cm/600s. Tests on these two older ages also included post-peak unloading cycles initiated at 30% and 60% of P_{max}; these data are not relevant to the present work.

3. Data Reduction and Results

Two categories of experimental results were obtained: (1) direct measurements of loads, displacements, and strains, and (2) inverse extrapolations of mechanical and fracture properties.

3.1. Directly Measured Quantities and Data Processing

The primary measurements were load and CMOD. (Load-point displacement measures were compromised by uncertainty in isolating the actual load-point displacement from the measured actuator stroke displacement, and are therefore not utilized in the analysis.) Both the load and CMOD measures were corrected to compensate for minor sources of variation. Assuming plane-strain conditions, load data were adjusted by a multiplicative factor to compensate for differences in specimen depths introduced by sawing. On the system level, contributions made by creep in the CMOD mounts were removed from the total measured CMOD data by utilizing the stage-2 creep rate that was measured before the initiation of loading. At this stage – before data condensing – the Young's modulus (E) and modulus of rupture (R) were computed, as described in section 3.2.

Further data processing was conducted to facilitate the extrapolation of fracture properties. The objective was to create a single load versus CMOD curve for each age of the reproduced Imperial mortar. Three steps were taken.

First, the specimen data sets were truncated to impose a uniform-stop condition. Most of the arc-shaped specimens did not fully separate along a through-going rupture. Rather, the fracture that propagated from the internal arc of the axial zone (fig. 1b) transformed the mechanical functionality of the specimens from that of a curved beam to an arch, whose action produced a compression-dominant zone in the upper 5-10% of the central ligament at the outer diameter (fig. 1b). This made the end-point of the test somewhat arbitrary, as the arching action permitted continued CMOD increase at extremely low loads. The criterion for a uniform stop was chosen as a loss of carrying capacity, κ_{cc}, defined as the ratio between the specimen's last measured load and its peak load

$$\kappa_{cc} = P_{stop} / P_{max} \tag{1}$$

This measure was selected to ensure that each specimen response had an identical test 'duration' in terms of the most relevant indicator, bearing capacity. The largest κ_{cc} from each chronological set dictated the truncation of the other seven, so that each specimen data set featured exactly the same loss of carrying capacity.

Next, an automated simplification routine was developed to reduce the total number of points in each specimen's data set to an identical number. The program followed the approach presented in [20], whereby the set is divided into the specified number of neighborhoods whose data points are averaged to a single group of values. In this way, each data set was condensed from about 10,000 to exactly 50 points, evenly divided about the pre- and post-peak applied load. The simplification process exactly preserved the data associated with the three points: the first non-trivial data point, the peak load, and the last data point (as given by the uniform-stop condition).

Lastly, each of the fifty data points from the eight specimens were averaged together to create that age's average response (the solid lines in fig. 4). These three curves, representing the 28-, 90-, and 180-day responses, were then utilized in the inverse determination of traction-separation descriptions for each age of reproduced Imperial mortar, as detailed in section 3.3.

3.2. Inverse Extrapolation of Mechanical Properties

3.2.1. Young's Modulus

Values for the Young's modulus (E) of each specimen were determined from the measured data between $0.1P_{max}$ and $0.4P_{max}$ in the load versus CMOD response, where P_{max} is the peak load (table 2). This range was identified to isolate the predominantly linear portion of the response, which was characterized by the stiffness K_{exp} [N/m], determined by a linear fit. A Finite Element Analysis (FEA) model of the experiment (fig. 3) with linear-elastic behavior for the reproduced mortar provided the constant deformability ratio, ξ [m^{-1}], between the input Young's modulus of the material model (E_{FEA}) and the output simulated K_{CMOD_FEA}

$$\xi = E_{FEA} / K_{FEA} \quad (2)$$

Each specimen's experimentally measured Young's modulus, E_{exp}, was then found by applying the deformability ratio to its measured stiffness

$$E_{exp} = \xi K_{exp} \quad (3)$$

These inversely computed Young's modulus values (E, table 2) were independently verified via the measured circumferential strains. The mean value, ε_{avg}, of the strain measured experimentally by the two gauges (ε_0 and ε_1, table 2, fig. 3) at a load of $0.4P_{max}$, was compared with the numerically computed strain from the FEA model, ε_{FEA}. This latter value was computed as the average circumferential strain in the band of elements (fig. 3) that approximately coincided with the location of the strain gauges during the experiments. The percent difference (%Diff, table 2) references the experimental values.

3.2.2. Modulus of Rupture

Values for each specimen's modulus of rupture (R) were found using the same numerical model. The model was defined using the specimen's previously extrapolated E and loaded with its experimentally measured P_{max} (table 2). The value for R (table 2) was computed as the mean circumferential stress in the center-most elements of the axial zone (fig. 3) when the specimen's full load (P_{max}) had been applied in the FEA model. This computation process was similar to that stipulated in [21], but with the closed-form bending formula expression for R replaced by an FEA calculation of the tensile stress at peak load.

3.3. Inverse Extrapolation of Fracture Properties

Fracture properties were determined via an iterative usage of FEA within a design-of-experiments (DOE) framework. This approach was adopted to mitigate the lack of directly measured fracture properties. There was insufficient experimental material to create specimens for splitting tests [22] to estimate uniaxial tensile strength (f_t), while a measure of the fracture energy (G_F) via the work-of-fracture method [18] was unavailable due to the arching action that impeded through-going fractures. The DOE approach was thus necessary to organize the variation in all four parameters of an assumed bilinear traction-separation description (TSD, fig. 5a): f_t, G_F, and the kink stress (σ_k) and displacement (w_k). This method enabled the creation of a response surface that identified the best-fit TSD for each age of the reproduced mortar. It also provided a practical resolution to the issue of solution uniqueness by ruling out all other physically admissible configurations. A limited volume of volcanic ash aggregate did not allow for testing of different sized/shaped specimens, which would have enabled a more formal verification of uniqueness.

The computational DOE arrays were informed by a sensitivity study that explored the effect of variations in each of the TSD parameters in results produced by FEA simulations of the experiment. The following four tendencies were identified: (1) increase in f_t increased only P_{max} and not its associated displacement, $CMOD(P_{max})$ (fig. 5b), (2) increase in G_F increased both P_{max} and $CMOD(P_{max})$ while also inducing a general 'rounding out' of the output load-CMOD response (fig. 5c), (3) increase in the relative stress retention ($\psi = \sigma_k / f_t$) produced a larger P_{max} (fig. 5d), and (4) increase in the relative displacement retention ($\zeta = w_k / w_f$, with w_f the displacement at complete separation (fig. 5a)) generated larger post-peak softening loads (fig. 5d).

A composite measure of the mean error between the experimental and simulated load versus CMOD curves was used as the characteristic response. The *average* percent difference, with the experimental curve as the reference, was calculated in terms of both load and CMOD at six points (fig. 6): peak load, final CMOD, and 0.1α, 0.25α, 0.5α, and 0.75α, with $\alpha = CMOD_{final} - CMOD(P_{max})$. The absolute values of the twelve relative error measures (six in load, six in CMOD) were combined in an un-weighted average to produce the mean error of that simulation.

All FEA simulations of the experiment were run in Abaqus. The softening model was a two-dimensional plane strain model that included four material definitions. Three were linear-elastic and modeled with plane-strain Incompatible Modes CPE4I elements: HDPE for the plastic CMOD mounts, steel for the foot-plates, and the bulk response of the reproduced mortar. The fourth was the TSD response of 75 cohesive linear-displacement COH2D4 elements embedded in the central ligament. Their behavior was governed by a penalty stiffness E_p=100GPa and a tabular definition of the separation displacement, w_s, as a function of a scalar damage parameter, D_s. The expression

$$w_s = w_s(D_s) = \begin{cases} \dfrac{f_t\ (D_s - 1)w_0 + D_s w_k\ + \sigma_k w_0}{f_t - (D_s - 1)E_p(w_0 + w_k) - \sigma_k}; & w_s < w_k \\ -\dfrac{(D_s - 1)f_t(w_f - w_k) + \sigma_k w_f}{(D_s - 1)E_p(w_f - w_k) - \sigma_k}; & w_s > w_k \end{cases} \quad (4)$$

enabled the automated definition of this table, with w_f the final displacement, σ_k the kink stress, w_k the kink displacement, and $w_0 = f_t / E_p$ the pseudo-elastic displacement; see [23,24] for further details on the implementation.

A sufficiently accurate TSD was defined as one with mean error less than 5%. If, following completion of the experimental array, an accurate TSD had not been identified, further optimization was conducted according to tendencies observed in the sensitivity study. In this way accurate TSDs were determined for each of the three hydration ages of the reproduced Imperial mortar (fig. 4). Mechanical and fracture properties appear in Table 3 and are discussed below.

4. Discussion of Results

4.1. Young Modulus and Modulus of Rupture

Results for E are validated internally using the measured strains. Comparison in table 2 between measured (ε_{avg}) and computed (ε_{FEA}) circumferential strains reveals a relatively good agreement (%Diff) for the 180- and 90-day specimens. Discrepancies of around ±15% are attributed to the proximity in size between the reproduced mortar's coarse volcanic ash particles (d_{max} = 0.64cm; see also Table 1) and the measuring length (l_g = 1.27cm) of the strain gauges. The homogeneous

FEA material model did not represent these local heterogeneities in the material microstructure, which could have affected the strain gauge readings. This effect is exacerbated in the 28-day specimens. The younger specimens were less coherent, so that gauges were often adhered to the rough surfaces of stiffer volcanic ash particles, which effectively stiffened the measured local strain response. Such difficulties would likely be avoided when testing a cementitious material that hardened more rapidly.

Results for both E and R are validated externally with data from the testing program of Samuelli Ferretti [11,25], which tested a slightly different Imperial-type mortar formulation, also using Pozzolane Rosse volcanic ash. For the 90- and 180-day specimens, the indirect measures of E via the present arc-shaped three-point bending scheme agree remarkably well with Sameulli Ferretti's direct measurements of E via compression tests: mean values of 2.90 and 3.37 GPa (Table 3) as compared to 2.96 and 3.24 GPa [25]. The 28-day results do not agree: the 3.43GPa measured by Samuelli Ferretti [25] is much larger than the 1.00GPa indirectly measured presently. However, Samuelli Ferretti's 28-day measure of E also exceeded his own 90- and 180-day measures for the same property (see above), suggesting that he, too, encountered a complex curing process.

Comparisons for R reveal a similar agreement. The 90- and 180-day flexural strengths from the present arc-shaped specimens show good correspondence with those strengths calculated by Samuelli Ferretti, who tested small prismatic beams in three-point bending and used the classical bending formula to compute R from the measured peak loads. The presently measured values for R of 1.09 and 1.35 MPa (Table 3) for the 90- and 180-day ages, respectively, compare well with the 1.32 and 1.02 MPa measured for the same ages by Samuelli Ferretti [25]. The 28-day flexural strength again reveals a larger difference: Samuelli Ferretti's value of 1.31MPa [25] substantially exceeds the 0.19MPa measured indirectly here.

The large discrepancies in the mechanical properties of the 28-day old mortars are perhaps attributable to differences in the grain size distributions of the volcanic pozzolan as well as the storage and curing conditions between the two experimental programs. Samuelli Ferretti's program used Pozzolane Rosse volcanic ash particles smaller than 2mm from a single quarry, while the present study included grain sizes more than three times larger, in an ash mix from

multiple quarries, in order to more accurately represent the mix design of the Markets of Trajan wall mortar. Furthermore, Samuelli Ferretti's program immersed specimens in a lime-saturated bath for curing, while the present study sealed the ends of the casting molds, in order to approximate the hydration conditions of the ancient mortars within the thick, brick-faced bearing walls of Imperial constructions. It is possible that the smaller grain-size fraction, which increased the reactive surface area of the Pozzolane Rosse ash relative to the natural grain size distribution, and the lime-saturated curing environment together accelerated hydration processes, accounting for the stiffer and stronger (in flexure) behavior of Samuelli Ferretti's 28-day old mortar. Ongoing chemical and mineralogical studies of our own Imperial mortar reproductions will clarify the curing processes and their effect on the development of mechanical properties.

Nevertheless, the consistency between the findings for the Young's modulus and modulus of rupture for the 180- and 90-day specimens is reassuring. The good agreement, notwithstanding variations in specimen geometries, materials, and curing conditions, suggests that the inverse process utilized in the present study is able to effectively identify the material/structural properties from the experimental response of the mortar specimens.

4.2. Traction-Separation Description

The softening results contribute new insight into the fracture behavior of Imperial Roman mortar. There are no comparable published results for the fracture properties available for reconciliation. Instead, modern concrete fracture mechanics concepts are consulted to provide some context for interpreting the experimental results.

First, the results of the inverse analysis are examined. The best-fit traction-separation descriptions (TSDs) accurately follow the experimental response (fig. 4). Fracture energy G_F increases with curing duration (Table 3), although its rate of increase with respect to that observed for several mixes of modern concrete in similar curing conditions [26] suggests a rather longer hardening process for the reproduced Imperial mortar. The uniaxial tensile strength f_t also increases with curing duration, while its ratio with the modulus of rupture R remains approximately constant (Table 3). These ratios, which average 2.3, are larger than those observed for modern concretes via standardized test protocols [27]. The disparity is likely due to the relatively small ratio of span:thickness, which induces a transverse shear contribution to the

structural stiffness and results in the overestimation of R. This could be further explored by testing of standard prismatic specimens [21].

The kink-point co-ordinates also evolve, with the relative stress retention (ψ) decreasing and the relative displacement retention (ζ) increasing with curing duration. The evolution of the TSDs during curing is probably attributable to the 'homogenization' that the reproduced Imperial mortar undergoes as the volcanic ash aggregate particles are incorporated into the composite material fabric by an increasingly coherent matrix. As the bond between binder and aggregate strengthens, a propagating macrofracture creates fewer bridging ligaments around the larger particles, decreasing the residual load-carrying capacity. This is visible in the diminishing of the relative stress retention ψ. Microstructural studies of the hydration processes and bonding within the mortar specimens will be described in a future publication.

A helpful quantitative description of the fracture process zone can be made using Hillerborg's characteristic length [28]. Written

$$_{ch} = \frac{E\ G_F}{f_t^2} \tag{5}$$

it estimates the ductility of a cementitious material and offers further insight into the evolution of the heterogeneous microstructure. The characteristic length decreases by more than 20% between the 28- and 90-day sets, and remains roughly constant between the 90- and 180-day sets (Table 3). The initial decrease in length reflects a more brittle response, consistent with the increased cohesion of the mortar's microstructural fabric – in particular the cementitious matrix – as it cures. The characteristic lengths at all three ages are fairly large with respect to modern concretes: a typical value for a modern structural concrete after 28 days hydration is about 400mm, based on an E = 25GPa, G_F = 150J/m^2, and f_t = 3MPa. By comparison, the reproduced Imperial mortar, even after 180 days, is more ductile.

The added presence of the dm-sized coarse aggregate (fig. 1), which expands the scale of heterogeneity by up to an order of magnitude in the ancient composite concrete, could further increase what is already a fairly ductile cementitious material. This perhaps alludes to one facet of the vaulted monuments' survival: the capability of the ancient concrete to absorb large

amounts of energy in sizable fracture process zones, without advancing structural-scale discontinuities [8,9,13].

4.3. Broader Discussion of the Experimental Program

The arc-shaped three-point bending test system was conceived to maximize the amount of fracture-mechanical information obtainable from testing the hollow cylinders of ancient Roman concrete core-samples from the Great Hall of the Markets of Trajan (fig. 1a). The testing of the reproduced Imperial mortar specimens served two purposes: to measure the mortar's fracture properties, and to 'benchmark' the test system to fully ensure a productive future usage of the unique and extremely rare ancient material.

The results presented here indicate that innovative test system makes effective and informative use of test material, in this the case reproduced Imperial mortar, although some improvements are recommended. The various 'material' properties are inversely computed rather than directly measured. These values should be validated – where possible – with directly measured results for independent response quantities. For this initial usage of the system, however, only the Young's modulus results were validated in this manner, via the strain gauge measurements. For the softening results there are no independently measured quantities available.

Two modifications to the test system are proposed to increase the number of directly measured quantities available for such an independent validation. First is the addition of crack propagation strain gauges mounted to vertically traverse the outer surfaces of the specimen. These gauges could digitally track the vertical propagation of the macrofracture on the outer surface of the specimen as it progresses through the ligament. These data would be readily compatible with FEA simulations.

Second is a more accurate measure of the load-point displacement. The problems in isolating the actual load-point displacement from the actuator extension can be corrected by a number of available methodologies, including the use of a regularizing cement such as hydrostone to cap the specimen footprints. This would improve pre-peak load-displacement measurements by ensuring perfectly smooth contact between the specimen and the staging footplates, thus allowing the stroke displacement to provide a more accurate specimen-scale measurement.

These additional measurements would provide a more rigorous verification of the uniqueness of the softening results. The present use of the design-of-experiments approach in the inverse process mitigated this condition to a degree, with the numerous possible configurations that it required to be tested permitting an argument to be made by refutation. That is, instead of affirming the measured properties as correct, the method determined all other physically admissible values to be incorrect. This approach is considered valid so long as two requirements are fulfilled. First, the experimental array must be defined to include all physically admissible values for the fracture properties at an appropriate resolution. Second, the array should identify only one single optimum configuration. If multiple optimum solutions are found, then an alternative approach must be adopted. Both requirements were satisfied for the three ages of reproduced Imperial mortar described here.

Other potential changes do not involve the test system. The size effect phenomenon, for example, has been found to affect measurements of the fracture energy [29]. While the present study focused on obtaining a first and statistically significant assessment of the reproduced Imperial mortar's fracture properties, future testing should consider specimens with carefully controlled variations in depth. It would also be informative to test larger-scale specimens, such as a full-sized structural element, as a larger-sized specimen would likely produce a more accurate characterization of the extended tail of the post-peak softening response. Finally, the testing procedure should be adjusted to include a pre-peak and additional post-peak unloading loops. The pre-peak unloading loop would provide an improved load-point displacement measure that is unaffected by crushing of uneven material in the specimen footprints, while the additional post-peak unloading loops would perhaps provide some insight into determining the damage coefficients for use in damaged-elasticity models [8].

5. Conclusions

An innovative experimental test program of a reproduced Imperial Roman mortar provides a detailed description of the mortar's composition, including a precise water content, a measure of the volume reduction of the lime paste during hydration, and a complete grain size distribution of the volcanic ash pozzolan mix. Novel casting mold designs are also described, along with the casting and curing procedures.

A new test system, the arc-shaped three-point bend test, is introduced. The experimental system is shown to accurately measure the load versus CMOD response throughout the fracture process of the arc-shaped specimens, which generally do not completely rupture due to arching action along the outer perimeter of the specimen. Two inverse FEA procedures measure mechanical and fracture properties, and reveal that the reproduced Imperial mortar undergoes a significantly longer hardening process than modern cementitious materials. All mechanical and fracture properties increased with age, and after 180-days curing, the reproduced Imperial mortar had Young's modulus and uniaxial tensile strength around one-tenth those of a modern concrete, while the fracture energy was roughly half. Together these properties indicate a relatively ductile cementitious material. Understanding the toughness of Imperial mortar, and by future extension Roman concrete, constitutes a critical step towards understanding the enduring structural successes of ancient Roman vaulted monuments and identifying possible applications towards extending the service lives of modern concrete structures formulated with volcanic ash pozzolans.

Acknowledgements

We gratefully acknowledge the generous assistance of Tim Bond in the Winter Lab at Cornell University for realizing the experimental setup and for innumerable helpful suggestions. Carmeuse Lime, in particular Kevin Smith, Mike Schrock, Carl Laird, and Dale Andrews, generously provided quicklime and invaluable expertise. This research would not have been possible without the collaboration of Lucrezia Ungaro and Massimo Vitti at the Sovraintendenza ai Beni Culturali del Comune di Roma, Ufficio Fori Imperiali, who also provided the all-important ancient core-samples. The Department of Mechanical Engineering at University of Rochester provided financial support for several aspects of this work.

References

[1] Samuelli Ferretti, A. 2005. Le Strutture Della Basilica. *La Basilica di Massenzio*. C. Giavarini. Roma, «L'Erma» di Bretschneider.

[2] Mark, R. and P. Hutchinson 1986. "On the Structure of the Roman Pantheon." *The Art Bulletin* **68**(1): 24-34.

[3] Giovannoni, G. 1931. "Contribuiti allo studio della tecnica nelle costruzione romane." *Atti del Congresso Nazionale di Studi Romani* **2**: 281-294.

[4] Tosi, A. 1997. "Un Esempio di Analisi Strutturale." *Materiali e Strutture* **7**(2-3): 122-130.

[5] Lancaster, L. C. 2005. *Concrete Vaulted Construction in Imperial Rome*. New York, Cambridge University Press.

[6] Heyman, J. 1966. "The Stone Skeleton." *International Journal of Solids and Structures* **2**: 249-279.

[7] Heyman, J. 1969. "The Safety of Masonry Arches." *International Journal of Mechanical Sciences* **11**: 363-385.

[8] Brune, P. F. 2010. *The Mechanics of Imperial Roman Concrete and the Structural Design of Vaulted Monuments*. Rochester, NY, University of Rochester. **Ph.D. Thesis**.

[9] Brune, P. F.*, et al.* 2010. The Toughness of Imperial Roman Concrete. *FRAMCOS7*. B.-H. Oh and K. Choi. Jeju, South Korea.

[10] Brune, P. F. and R. Perucchio 2011. "Numerical Simulation of the Mechanical Behavior of Opus Caementicium: Opportunities and Challenges." *Commentationes Humanarum Litterarum Series* **128**: 96-108.

[11] Samuelli Ferretti, A. 1996. "Materiali da costruzione e tecnologie costruttive del patrimonio archeologico e monumentale romano con particolare riferimento al tipo laziale ed all'opus latericium." *Unpublished research conducted at Università degli Studi di Roma "La Sapienza" - Dipartimento di Ingegneria Strutturale e Geotecnica*.

[12] Lamprecht, H.-O. 1984. *Opus Caementitium*. Düsseldorf, Beton-Verlag.

[13] Jackson, M. D.*, et al.* 2009. "Assessment of material characteristics of ancient concretes, Grande Aula, Markets of Trajan, Rome." *Journal of Archaeological Science* **36**: 2481-2492.

[14] Ungaro, L., M. P. Del Moro, and M. Vitti, 2010, *I Mercati di Traiano Restituiti*, Rome, Palombri Editori.

[15] Jackson, M. D.*, et al.* 2010. "Mid-Pleistocene volcanic ash in ancient Roman concretes." *Geoarchaeology* **25**: 36-74.

[16] ACI-Committee446 2010. Fracture Toughness Testing of Concrete, Draft.

[17] Elices, M., et al. 2002. "The cohesive zone model: advantages, limitations and challenges." Engineering Fracture Mechanics **69**: 137-163.

[18] RILEM 1985. "Determination of the fracture energy of mortar and concrete by means of three-point bend tests on notched beams." Materials and Structures **18**(106): 285-290.

[19] Granger, F., 1931. Vitruvius On Architecture, Books I–IV (translator). Harvard University Press, Cambridge (reprint 2002).

[20] Zhao, Z., S. H. Kwon and S. P. Shah 2008. "Effect of specimen size on fracture energy and softening curve of concrete: Part I. Experiments and fracture energy." *Cement and Concrete Research* **38**: 1049-1060.

[21] ASTM C293 2002. Standard Test Method for Flexural Strength of Concrete (Using Simple Beam With Center-Point Loading). West Conshohocken, PA, American Society of Testing and Materials.

[22] ASTM C496 2004. Standard Test Method for Splitting Tensile Strength of Cylindrical Concrete Specimens. West Conshohocken, PA, American Society of Testing and Materials.

[23] Roesler, J.*, et al.* 2007. "Concrete fracture prediction using bilinear softening." *Cement and Concrete Composites* **29**: 300-312.

[24] Dassault Systèmes 2009. *Abaqus User's Manual v6.9*. Providence, RI, Simulia.

[25] Giavarini, C., A. Samuelli Ferretti and L. Santarelli 2006. Mechanical Characteristics of Roman 'Opus Caementicium'. *Fracture and Failure of Natural Building Stones*. S. Kourkoulis. Dordrecht, Springer.

[26] Kim, J.-K., Y. Lee and S.-T. Yi 2004. "Fracture characteristics of concrete at early ages." *Cement and Concrete Research* **34**: 507-519.

[27] Raphael, J.M. 1984. “Tensile Strength of Concrete.” *American Concrete Institute Journal, Proceedings* **81**(2): 158-165.

[28] Hillerborg, A., M. Modéer and P. Petersson 1976. "Analysis of crack formation and crack growth in concrete by means of fracture mechanics and finite elements." *Cement and Concrete Research* **6**: 773-782.

[29] Bažant, Z. P. and J. Planas 1998. *Fracture and Size Effect in Concrete and Other Quasibrittle Materials*. Boca Raton, CRC Press.

Figure captions

Fig. 1. Photographs of (a) 2000-year-old concrete from the Markets of Trajan (*c*. 110AD) and (b) a reproduction of its volcanic ash-hydrated lime mortar. The 20cm-diameter drill core of ancient wall concrete has large clasts of volcanic tuff and brick coarse rubble aggregate surrounded by a compact pozzolanic mortar. The post-fracture experimental mortar specimen shows a typical fracture propagation from the axial zone towards the outer diameter, and represents one-half of a 7cm-deep slice of the drill core, which will be tested using the same arc-shaped three-point bending test.

Fig. 2. Schematic of test specimen, showing (a) HDPE CMOD mounts, (b) steel loading helmet, and (c) circumferentially oriented strain gauges.

Fig. 3. Left, three-dimensional FEA model showing load and CMOD measures. Right, locations of element bands used for computation of circumferential strains (top) and modulus of rupture (bottom).

Fig. 4. Comparison of experimental (solid) and computational (dashed) results for the three ages of reproduced Imperial mortar.

Fig. 5. (a) General bilinear traction-separation description (TSD) with various characteristic parameters, and the effects on the load-CMOD response by (b) changes to the uniaxial tensile strength f_t, (c) changes to the fracture energy G_F, and (d) curve form (kink point locations).

Fig. 6. The six points (providing twelve measures) on the load-CMOD curve used to compute the mean error in evaluating the accuracy of simulation results.

Table captions

Table 1. Natural grain size distribution of Pozzolane Rosse volcanic ash as utilized to control the mortar mix design. Weight % refers to the relative percentage in the mix of the Pozzolane Rosse particles retained by each sieve size.

Table 2. Experimental measurements for all specimens from the pre-peak regime with computations for Young's modulus E, modulus of rupture R, and validation with circumferential strain measures.

Table 3. Engineering and fracture properties as computed for the average response of each of the three mortar ages.

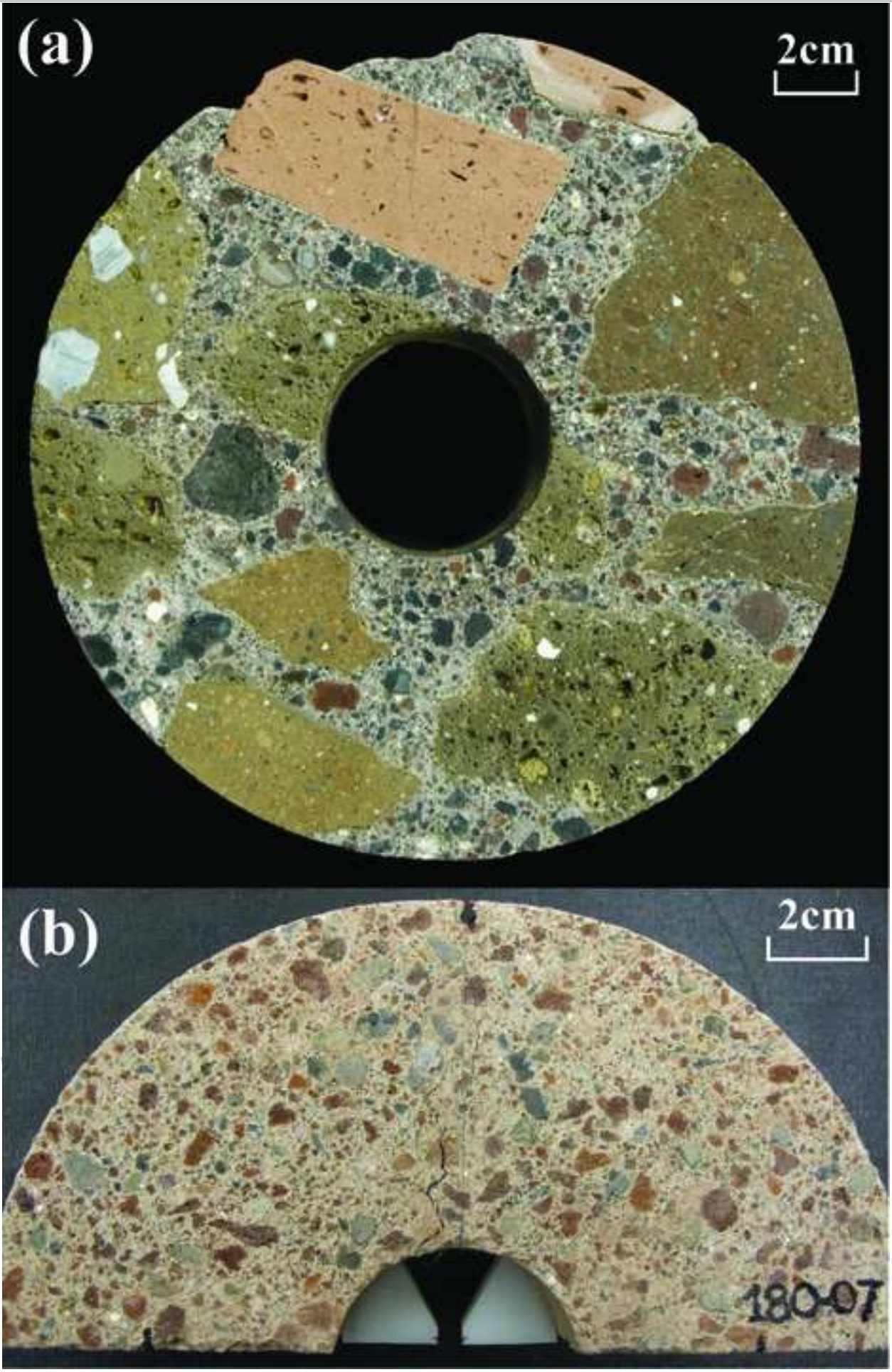

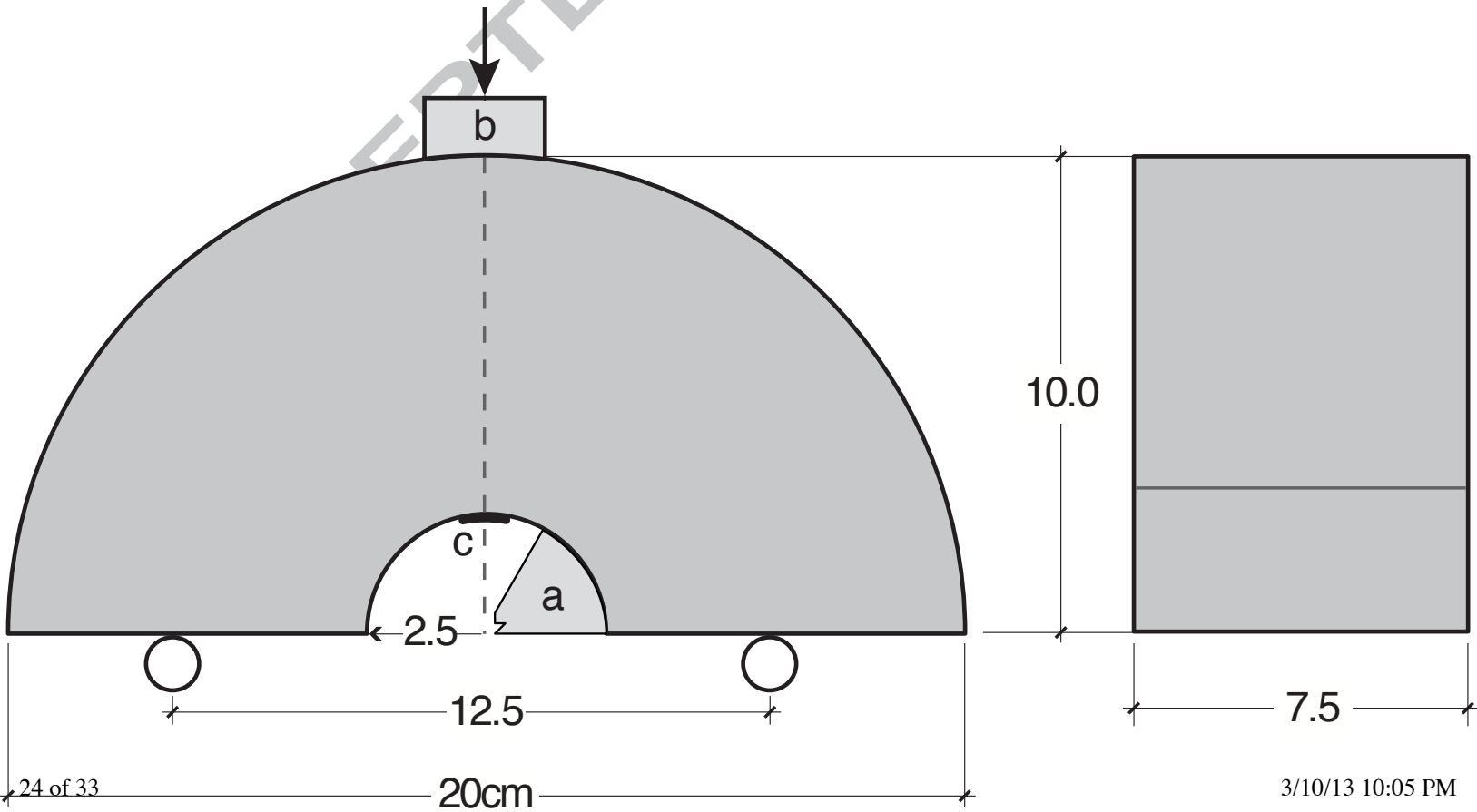

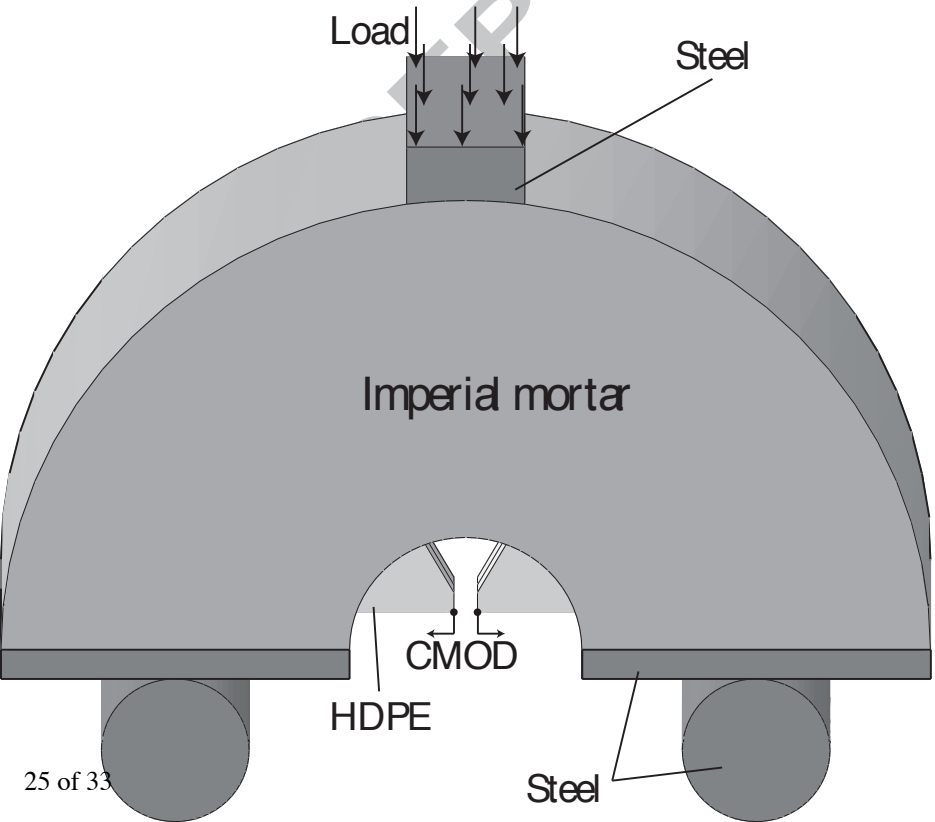

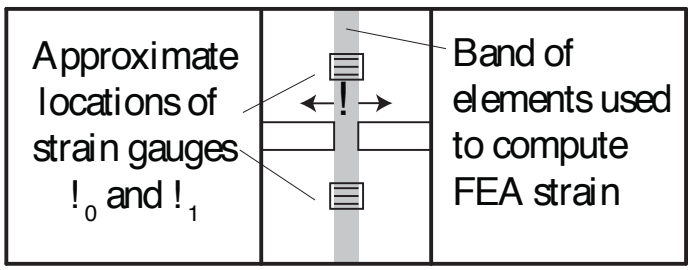

Bottom view

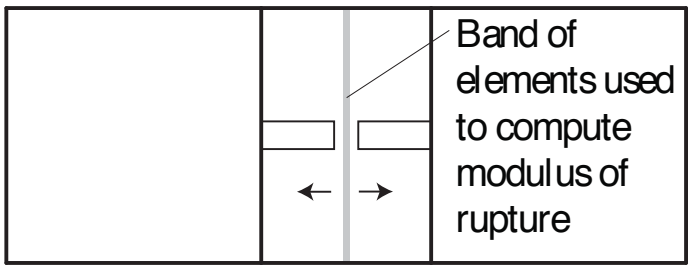

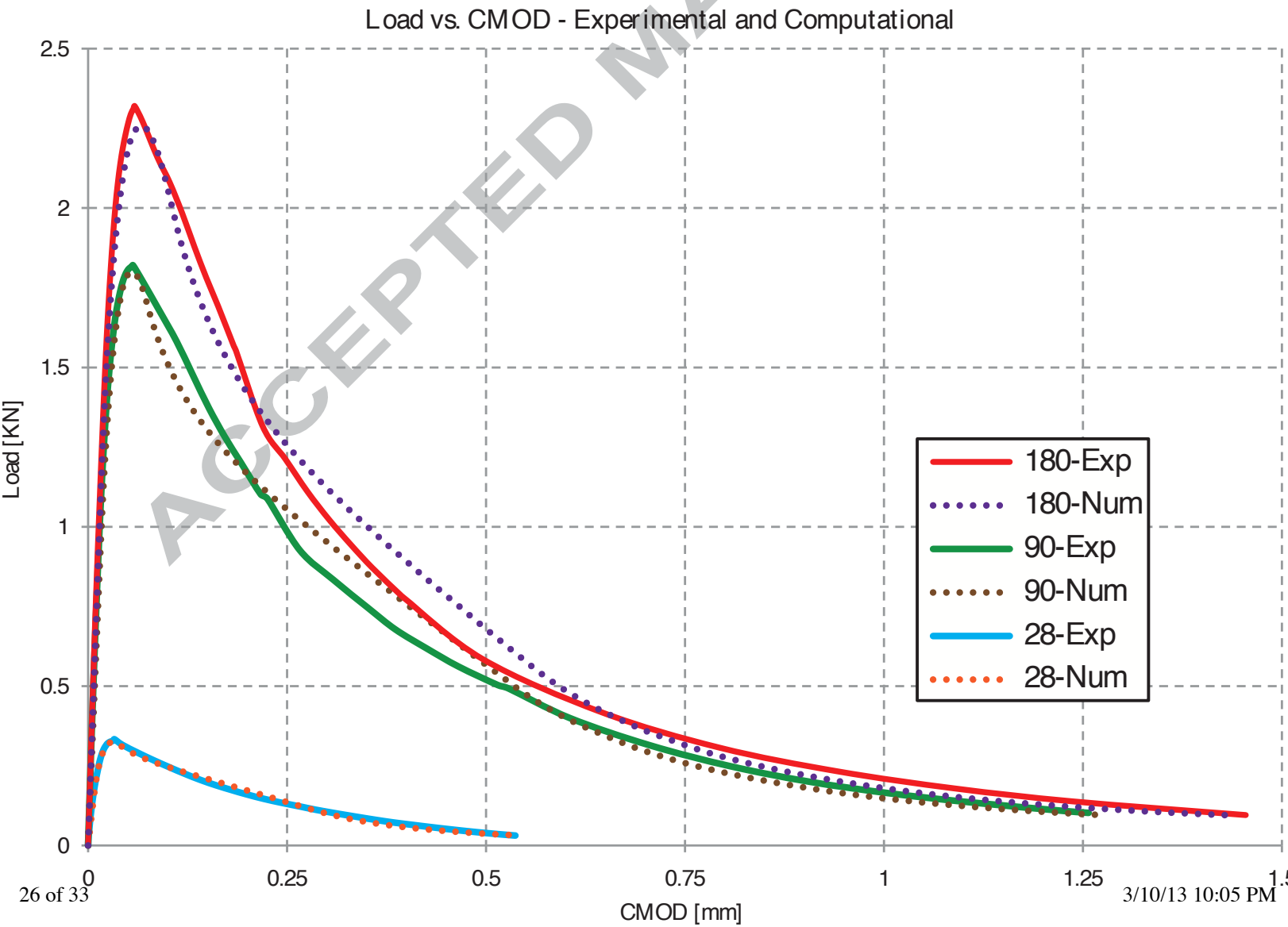

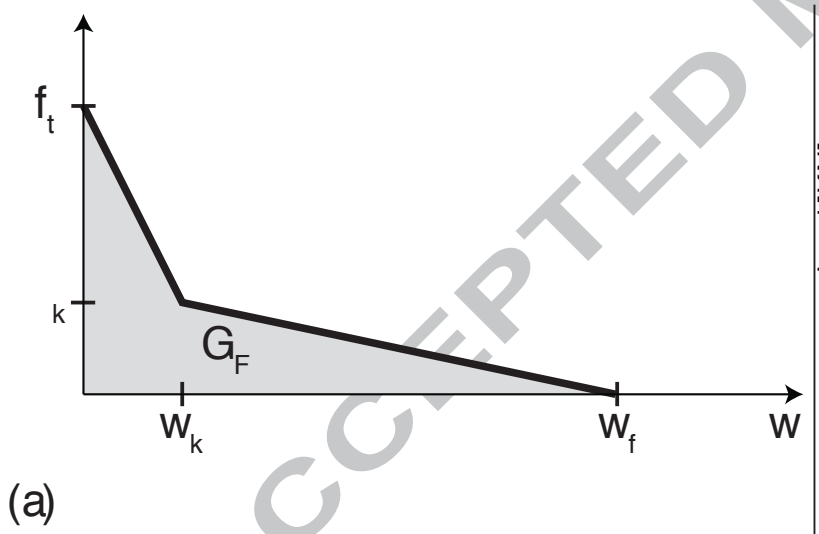

(a)

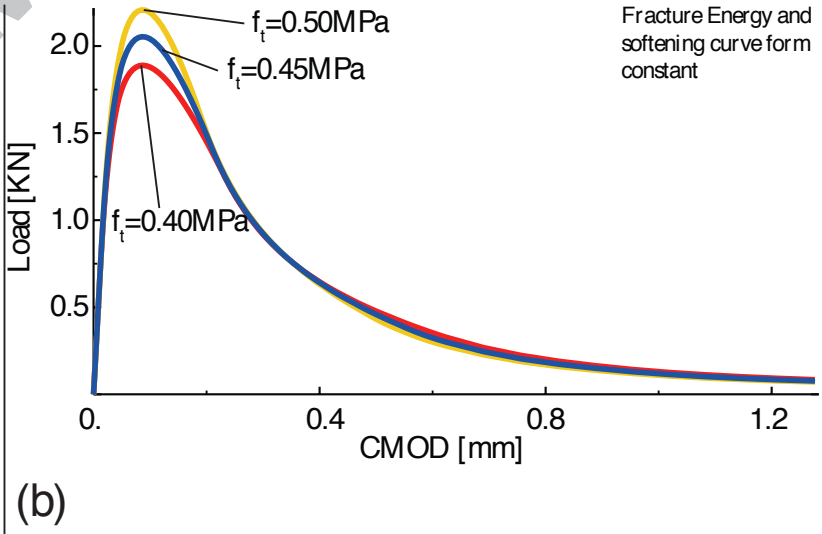

(b)

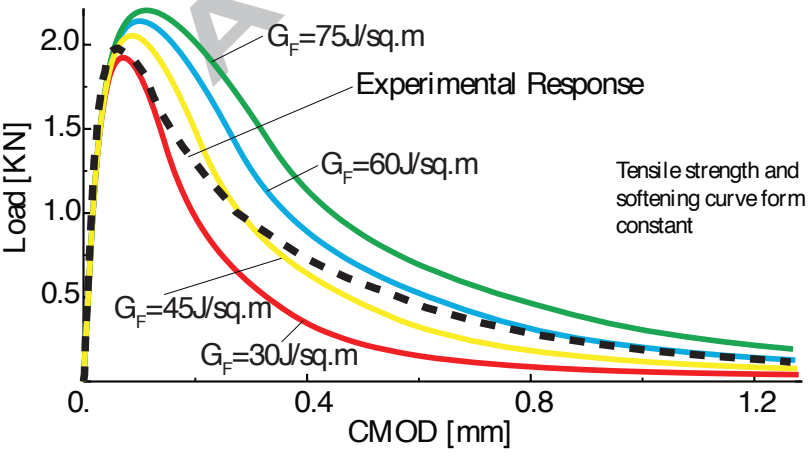

(c)

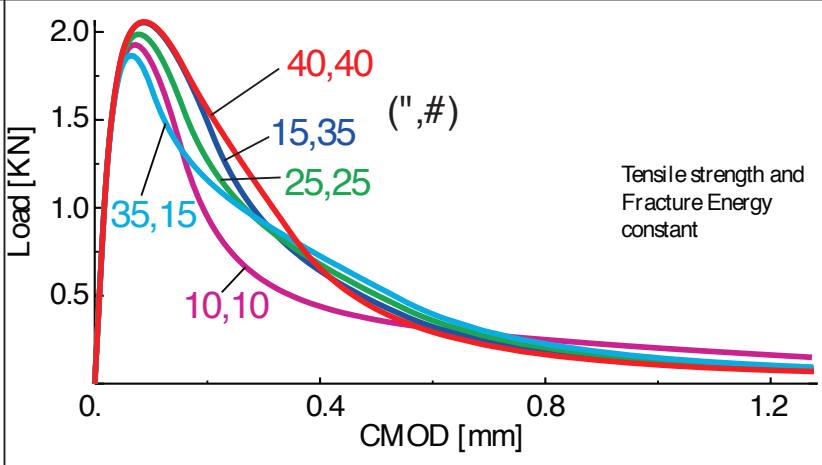

(d)

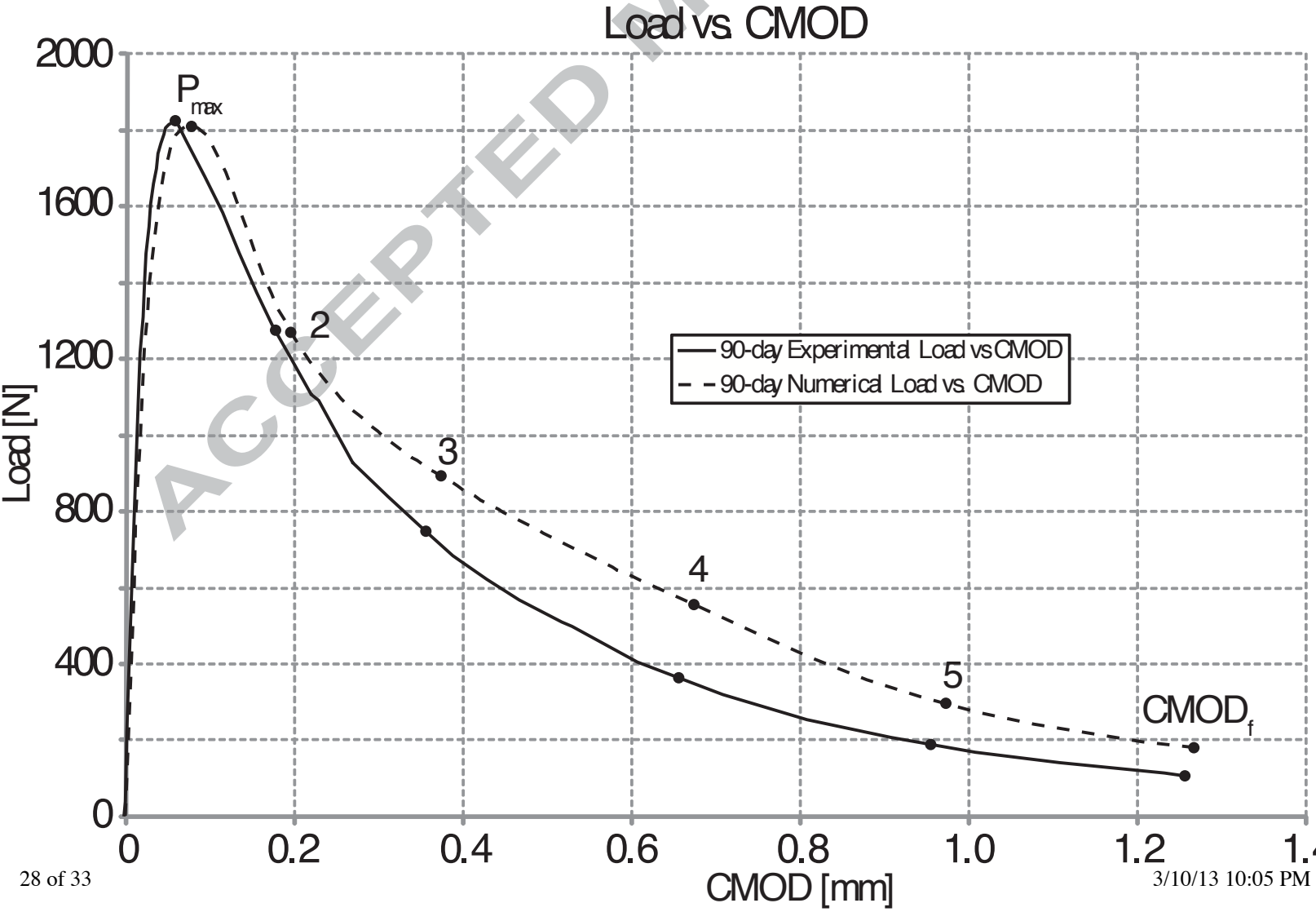

ASTM Sieve #	4	8	16	30	50	100	200	PAN
Weight %	26.7	18.75	15.34	10.8	9.66	9.66	6.25	2.84
Opening size [mm]	4.75	2.38	1.2	0.6	0.3	0.15	0.075	<0.075

Specimen	K_{CMOD} [N/mm]	P_{max} [N]	E [GPa]	R [MPa]	$_0$ [m]	$_1$ [m]	$_{avg}$ [m]	$_{FEA}$ [m]
180-01	117802	2589	5.32	1.4756	--	--	--	--
180-02	68216	2181	3.08	1.2438	0.134	0.215	0.175	0.152
180-03	62016	2033	2.80	1.1596	0.124	0.163	0.144	0.155
180-04	74601	2566	3.37	1.4634	0.145	0.097	0.121	0.162
180-05	82118	2512	3.71	1.4323	0.149	0.148	0.149	0.145
180-06	65798	2022	2.97	1.1531	0.134	0.072	0.103	0.145
180-07	61801	2149	2.79	1.2258	0.143	0.100	0.122	0.164
180-08	75685	2504	3.42	1.4279	0.134	--	0.134	0.156
180AVG	74579	2319	3.37	1.3239	0.135		0.135	0.157
90-01	77666	1986	3.51	1.1322	0.146	0.121	0.134	0.121
90-02	66242	1705	2.99	0.9722	0.075	0.142	0.109	0.122
90-03	75045	1740	3.39	0.9919	0.066	0.186	0.126	0.109
90-04	98198	2201	4.44	1.2545	0.134	0.104	0.119	0.106
90-05	69034	1833	3.12	1.0451	0.124	0.099	0.112	0.125
90-06	62189	1722	2.81	0.9820	0.105	0.160	0.133	0.131
90-07	64553	1703	2.92	0.9711	0.139	0.215	0.177	0.124
90-08	64040	1676	2.89	0.9557	0.111	0.085	0.098	0.124
90AVG	64227	1821	2.90	1.0381	0.126		0.126	0.119
28-01	27375	345	1.24	0.1970	0.054	0.052	0.053	0.059
28-02	17786	298	0.81	0.1704	0.045	--	0.045	0.079
28-03	18174	336	0.83	0.1921	0.041	0.049	0.045	0.087
28-04	18113	277	0.82	0.1584	0.030	--	0.030	0.072
28-05	25400	337	1.15	0.1925	0.020	--	0.020	0.063
28-06	23370	355	1.06	0.2028	0.036	0.066	0.051	0.072
28-07	21374	345	0.97	0.1972	0.071	0.021	0.046	0.076
28-08	27022	376	1.23	0.2147	0.102	0.067	0.085	0.065
28AVG	22327	334	1.01	0.1906	0.050		0.050	0.070

Age [Days]	E [GPa]	R [MPa]	f_t [MPa]	R/f_t	G_F [J/m^2]	[%]	[%]	l_{ch} [mm]
28	1.00	0.19	0.08	2.4	5	10	50	781
90	2.90	1.02	0.47	2.2	45	10	40	591
180	3.37	1.32	0.55	2.4	55	15	35	613

Nomenclature

CMOD	Crack Mouth Opening Displacement
E	Young's modulus
R	Modulus of rupture
κ_{cc}	Carrying capacity loss factor
P_{max}	Peak load
K_{exp}	Experimentally measured stiffness
ξ	Deformability ratio
E_{FEA}	FEA Young's modulus
K_{CMOD_FEA}	FEA stiffness
E_{exp}	Experimentally measured Young's modulus
ε_{avg}	Mean experimentally measured strain
ε_{FEA}	Numerically computed strain
G_F	Mode-I tensile fracture energy
f_t	Uniaxial tensile strength
σ_k	Kink stress
w_k	Kink displacement
ψ	Relative stress retention
ζ	Relative displacement retention
α	CMOD range
E_p	FEA penalty stiffness
D_s	Scalar damage parameter
w_0	Pseudo-elastic displacement
d_{max}	Size of largest aggregate particle in mortar mix
l_g	Measuring length of strain gauge

Highlights

First published test results of the fracture properties of an ancient material.

First published details of the mix design of Trajanic-era Roman mortar, a key part of history's most durable concrete.

First published details of a new test system to measure fracture properties, the arc-shaped three-point bend test.